

Dark Matter and HI in Ultra-Diffuse Galaxy UGC 2162

Chandreyee Sengupta,¹★ T. C. Scott², Aeree Chung³, O. Ivy Wong⁴

¹ Purple Mountain Observatory, No.8 Yuanhua Road, Qixia District, Nanjing 210034, China

² Institute of Astrophysics and Space Sciences (IA), Rua das Estrelas, 4150-762 Porto, Portugal

³ Department of Astronomy, Yonsei University, 50 Yonsei-ro, Seodaemun-gu, Seoul, Republic of Korea

⁴ International Centre for Radio Astronomy Research (ICRAR), University of Western Australia, 35 Stirling Highway, WA 6009, Australia

ABSTRACT

Our GMRT H I observations of the ultra diffuse galaxy (UDG) UGC 2162, projected ~ 300 kpc from the centre of the M 77 group, reveal it to have an extended H I disk ($R_{HI/R_{25}} \sim 3.3$) with a moderate rotational velocity ($V_{rot} \sim 31$ km s⁻¹). This V_{rot} is in line with that of dwarf galaxies with similar H I mass. We estimate an M_{dyn} of $\sim 1.14 \times 10^9 M_{\odot}$ within the galaxy’s $R_{HI} \sim 5.2$ kpc. Additionally, our estimates of M_{200} for the galaxy from NFW models are in the range of 5.0 to $8.8 \times 10^{10} M_{\odot}$. Comparing UGC 2162 to samples of UDGs with H I detections show it to have amongst the smallest R_e with its M_{HI}/M_* being distinctly higher and $g - i$ colour slightly bluer than typical values in those samples. We also compared H I and dark matter (DM) halo properties of UGC 2162 with dwarf galaxies in the LITTLE THINGS sample and find its DM halo mass and profile are within the range expected for a dwarf galaxy. While we were unable to determine the origin of the galaxy’s present day optical form from our study, its normal H I rotation velocity in relation to its H I mass, H I morphology, environment and dwarf mass DM halo ruled out some of the proposed ultra diffuse galaxy formation scenarios for this galaxy.

Key words: galaxies: ISM - galaxies: interactions - galaxies: kinematics and dynamics - galaxies: individual: UGC 2162 - radio lines: galaxies

1 INTRODUCTION

Since the discovery of forty seven ultra diffuse galaxies (UDG) in the Coma cluster by van Dokkum et al. (2015a), there have been several further reports of many more UDGs, mostly in galaxy clusters (e.g., Yagi et al. 2016; Wittmann et al. 2017; Toloba et al. 2018). UDGs have M_* of 10^7 to $10^8 M_{\odot}$, a central $g - i$ band surface brightness (μ_g) of > 24 mag arcsec⁻² and an effective radius (R_e) of $\sim 1.5 - 5$ kpc. UDGs are found in a range of environments from clusters and groups to in isolation, with their relative abundance increasing from the field to the centres of massive galaxy clusters (van der Burg et al. 2017). This implies a significant role for environment in the evolution at least some of them (Carleton et al. 2019). UDGs also display a wide range of properties from spheroids with red $g - i$ colours (~ 0.8) to irregulars with blue blue $g - i$ colours (~ 0.3) (Trujillo et al. 2017). While faint, extended, low surface brightness galaxies are not a recent discovery, the Coma UDGs revealed for the first time their relative ubiquity in a dense environment. Moreover, compared to classical LSBs, the Coma UDGs were fainter and often more extended (Yagi et al. 2016; van der Burg et al. 2017).

Despite the relatively large number of reported UDGs, little is

known about their properties and formation scenario(s). Currently some of the principal ideas put forward to explain UDG formation are: (1) galaxies with higher than average angular momentum and low star formation (Amorisco & Loeb 2016) (2) failed massive galaxies where either the environment or strong stellar feedback have suppressed star formation (SF) (van Dokkum et al. 2016; Di Cintio et al. 2017) (3) a subset of classical LSBs or are a class of dwarf galaxies following an evolutionary sequence from field to cluster as suggested by Yozin & Bekki (2015); Román & Trujillo (2017); Carleton et al. (2019), i.e., normal dwarfs spirals which have been converted to UDGs by an environmentally aided process/processes (e.g., star formation (SF) quenching, tidal heating, tidal stripping or ram pressure).

In this paper we present resolved Giant Metrewave Radio Telescope (GMRT) H I observations of UGC 2162, a UDG with $\mu_g \sim 24.4$ mag asec⁻², $R_e \sim 1.7$ kpc and a $g - i$ colour of 0.33 ± 0.02 (Trujillo et al. 2017). Table 1 gives a summary of the galaxy’s properties. Trujillo et al. (2017) showed that the stellar component of the galaxy consists of a elongated blue star forming region within a more extensive region of low surface brightness stellar emission. Using a redshift independent distance of 12.3 ± 1.7 Mpc for UGC 2162 it is claimed to be the nearest UDG (Trujillo et al. 2017), making it an excellent candidate for a resolved H I study. Being located in the IAC stripe82 Legacy Survey region, the galaxy has deep optical images. UGC 2162 is a member of the M 77 group and is projected ~ 294 kpc from the group’s centre. The nearest group

* e-mail: sengupta.chandreyee@gmail.com(CS)

¹ The effective radius of a galaxy is the radius at which half of the total light of the system is emitted.

Table 1. Properties of UGC 2162

Property ^a	Units	Value
$V_{radial(optical)}$ ^b	[km s ⁻¹]	1185±6
RA	[h:m:s]	02:40:23.09
DEC	[d:m:s]	+01:13:45.3
Distance ^c	[Mpc]	12.3 ± 1.7
R_e ^d	[kpc]	1.7±0.2
$\mu_g(0)$ ^e	[mag arcsec ²]	24.4±0.1
D ₂₅ major axis	[arcsec]	52
D ₂₅ major axis	[kpc]	3.2
Inclination ^f	[°]	55
Morphology		UDG
12+log(O/H) ^g		8.22± 0.07
M_* ^h	[10 ⁷ M _⊙]	2±2
M_{HI}	[10 ⁷ M _⊙]	18

^a From NED

^b From Hyperleda

^c See section 1.

^d From Trujillo et al. (2017).

^e From Trujillo et al. (2017).

^f From BBarolo fit to medium resolution GMRT H I cube.

^g For the brightest SF knot from a SDSS spectrum Trujillo et al. (2017).

^h From Trujillo et al. (2017).

member to UGC 2162 with comparable or greater stellar mass is SDSS J023848.50+003114.2 which is projected 48.7 arcmin (~ 175 kpc) away and separated in velocity by 277 km s⁻¹.

Section 2 gives details of the GMRT observations, with observational results in section 3. A discussion follows in section 4 with a summary and concluding remarks in section 5. In this paper we adopt the redshift to UGC 2162 of 0.00392 and distance to the galaxy of 12.3 Mpc from Trujillo et al. (2017). We also adopt their angular scale of 1 arcmin ~ 3.6 kpc. All α and δ positions referred to throughout this paper are J2000.0.

2 OBSERVATIONS

UGC 2162 was observed at 21 cm using the GMRT on the 8th March, 2018 and the observational parameters are detailed in Table 2. The GMRT data was analysed using the standard reduction procedures with the Astronomical Image Processing System (AIPS) software package. The flux densities are on the scale of Baars et al. (1977), with uncertainties of ~ 5%. After calibration and continuum subtraction in the uv domain the AIPS task IMAGR was used to convert the uv domain data to H I image cubes. Finally integrated H I, velocity field and velocity dispersion maps were extracted from the image cubes using the AIPS task MOMNT. To study the H I distribution in detail, image cubes with different resolutions were produced by applying different ‘tapers’ to the data with varying uv limits. Details of the final low, medium and high resolution maps are given in Table 2.

3 OBSERVATIONAL RESULTS

3.1 H I morphology and H I mass

Our UGC 2162 total intensity H I maps at low, medium and high angular resolution are shown in Figure 1, with the beam size and

Table 2. GMRT observational and map parameters

Rest frequency	1420.4057 MHz
Observation Date	8th March, 2018
Integration time	10.0 hrs
primary beam	24' at 1420.4057 MHz
Low resolution beam–FWHP	43.3'' × 39.3'', PA = 13.4°
Medium resolution beam–FWHP	30.7'' × 28.8'', PA = - 4.5°
High resolution beam–FWHP	16.9'' × 12.9'', PA = 31.7°
RA (pointing centre)	02 ^h 40 ^m 23.10 ^s
DEC (pointing centre)	01° 13' 45.01''

PA for each resolution given in Table 2 and indicated with white ellipses on the maps. At the distance of 12.3 Mpc, the low, medium and high resolution full width half power (FWHP) beams sample the galaxy’s H I disc at 2.6 kpc, 1.8 kpc and 1.0 kpc respectively. While the two lower resolution maps show regular H I morphology, the high resolution map reveals sub-structure, with the two principal H I maxima in that map having column densities of 1.0 to 1.2 × 10²¹ atoms cm⁻². Overall the outer H I disk morphology at all three resolutions is rather symmetric and shows no signs of extended tails or diffuse edge structures that would signify a recent interaction. From the low resolution H I map’s major axis we estimate the $R_{HI} \sim 86$ arcsec (~5.2 kpc), compared to the $R_{25} = 26$ arcsec (1.6 kpc) from Trujillo et al. (2017). Its R_{HI}/R_{25} is therefore ~ 3.3, i.e. almost twice the R_{HI}/R_{25} of ~1.8 typical of late-type galaxies (Broeils & Rhee 1997). Comparing the UGC 2162 R_{HI}/R_{25} to the morphologically unclassified Local Volume H I Survey (LVHIS Wang et al. 2017; Koribalski et al. 2018) sample (limited to galaxies with $M_* < 1 \times 10^8 M_\odot$), see Figure 3, indicates UGC 2162 lies within the upper range of R_{HI}/R_{25} for observed galaxies with $M_* < 1 \times 10^8 M_\odot$. We note that the faint, patchy optical disk revealed by the deep g, r, i IAC Stripe82 composite image, Figure 1 in Trujillo et al. (2017), extends to a radius of ~ 60 arcsec (3.6 kpc), i.e. more than twice the R_{25} .

In Table 3 and Figure 2 we compare the properties of the integrated GMRT H I spectrum with those from the 42m Green Bank Telescope (GBT, Springob et al. 2005) and Parkes Telescope Multi-beam (HIPASS Meyer et al. 2004) single dish spectra. Both the V_{HI} and W_{20} derived from the three radio telescopes are in agreement within their uncertainties. While we believe our measurement of the W_{20} from HIPASS spectrum is correct, Meyer et al. (2004) reported the W_{20} from the HIPASS spectrum as 89 km s⁻¹ and this is discussed in Section 4.1. The H I flux recovered by the GMRT interferometric observation ($S_{HI} = 4.5$ Jy km/s) is in good agreement the GBT absorption corrected flux ($S_{HI} = 5.1$ Jy km/s). Because it has the best signal to noise ratio (S/N) of the available spectra, we use the GBT flux to estimate the galaxy’s H I mass. This gives a $M_{HI} = 1.8 \times 10^8 M_\odot$ for the galaxy.

From the IAC Stripe82 deep observations (Trujillo et al. 2017) estimated the UGC 2162 g – band optical diameter $D_{25} \sim 52$ arcsec (3.2 kpc). Using this optical diameter, the $\log(M_{HI}/D_I^2)$ value for UGC 2162 is 7.24. The average value of $\log(M_{HI}/D_I^2)$ for galaxies of similar morphological type is 6.87 ± 0.17 (Haynes & Giovanelli 1984), indicating UGC 2162 is H I rich compared to other galaxies of similar size and morphological type. This conclusion is confirmed in Figure 4 which shows M_{gas}/M_* compared to M_* for UGC 2162, the LITTLE THINGS sample of dwarf galaxies² (Oh et al. 2015) and the morphologically unclassified LVHIS sam-

² for which M_* values available

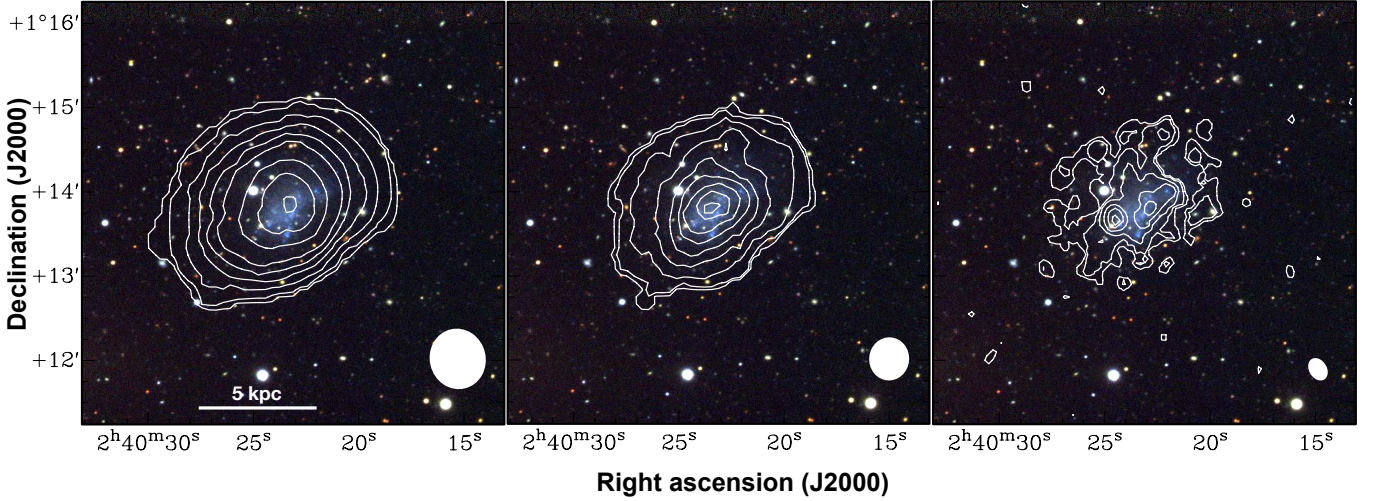


Figure 1. UGC 2162: left to right GMRT low ($43.3'' \times 39.3''$), medium ($30.7'' \times 28.8''$) and high ($16.9'' \times 12.9''$) resolution integrated H I map contours on SDSS g, r, i band composite image. The GMRT beam size and orientation is shown with white ellipses at the bottom right of each panel. **Low resolution contour levels:** 10^{20} atoms cm^{-2} (0.3, 0.7, 1.3, 1.9, 2.6, 3.2, 4.5, 5.6, 7.1) **Mid resolution contour levels:** 10^{20} atoms cm^{-2} (0.5, 0.9, 1.8, 3.1, 4.3, 5.6, 6.8, 8.1, 8.9) **High resolution contour levels:** 10^{20} atoms cm^{-2} (1.2, 2.5, 5.0, 7.5, 10.0, 12.6).

Table 3. UGC 2162 GMRT, GBT and HIPASS H I spectra properties

Telescope	Velocity ^a km s ⁻¹	W ₂₀ ^b km s ⁻¹	Channel width km s ⁻¹	(S)/N	S _{HI} Jy km/s
GMRT ^c	1185±2	49±5	6.9	5.6	4.5
GBT	1182±1	50±2	2.1	8.7	5.1 ^d
HIPASS	1178±2	53±4	13.4	6.4	5.4 ^e
Optical	1185±6				

^a Velocity = V_{HI} except for 'Optical' which is the optical velocity from NED.

^b Our measurement from the GBT and HIPASS spectra.

^c From the GMRT mid-resolution cube.

^d Self-absorption corrected, integrated flux density from (Springob et al. 2005).

^e From (Meyer et al. 2004).

ple for galaxies, but limited to members of both samples with $M_* < 1 \times 10^8 M_\odot$. For consistency with LITTLE THINGS, M_{gas}/M_* for UGC 2162 and LVHIS = $1.4 \times M_{HI}$, with the additional factor to account for molecular gas (0.04) and He (0.36). The figure shows that the M_{gas}/M_* ratio for UGC 2162 is 13.3, which is almost a factor of three higher than the median M_{gas}/M_* ratio for the LITTLE THINGS dwarfs of 4.7 and the mean of 4.6 ± 5.0 for LVHIS. The LITTLE THINGS outlier with $M_{gas}/M_* > 40$ is the well known super gas rich dwarf DDO154. Figure 4 also shows the mean M_{gas}/M_* ratio³ (7.18) from the 21 UDGs in the NIHAO simulation (Di Cintio et al. 2017). From the figure we see that the UGC 2162 M_{gas}/M_* ratio is higher than the mean of the simulated UDGs. (see also Figure 3). Overall our analysis suggests that UGC 2162 falls within the ranges of R_{HI}/R_{25} and M_{HI}/M_* observed in galaxies

with similar M_* in the THINGS and LVHIS samples, but displays amongst the highest M_{gas}/M_* ratios in its M_* range.

Figure 5 compares the M_{HI}/M_* v R_e and g-i color v R_e for UGC 2162 with those from samples of UDGs with H I single dish detections in ALFALFA (Leisman et al. 2017) and H I mapping (Spekkens & Karunakaran 2018). M_{HI}/M_* for UGC 2162 and the Spekkens sample was calculated using M_* from (Trujillo et al. 2017) and Spekkens & Karunakaran (2018) respectively. M_* was calculated for the Leisman⁴ sample using SDSS model magnitudes (g and i band) and parameters from Bell et al. (2003) and Blanton et al. (2003). Additionally, we calculated the SDSS g -

⁴ The full sample contained 115 UDGs but we excluded 19 UDGs with $M_{HI}/M_* \geq 80$. The 19 excluded UDGs are outliers in terms of M_{HI}/M_* with g band magnitudes in most cases ≥ 21 . These galaxies were excluded because the extreme M_{HI}/M_* raised questions about the reliability of their SDSS photometry for determining M_* .

³ $M_{gas} = M_{HI} \times 1.4$

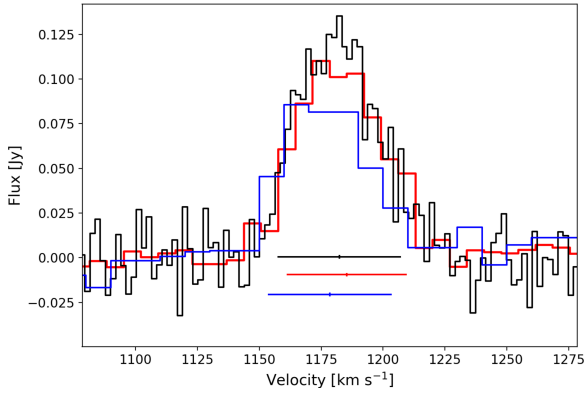


Figure 2. UGC 2162 H I spectra: GBT (black), GMRT (red) and HIPASS (blue). The channel widths of the GBT, GMRT and HIPASS spectra are 2.1, 6.9 and 13.4 km s⁻¹ respectively. The bars at the base of the spectra show the W_{20} of each spectrum in its respective colour.

i colours for all galaxies from their SDSS model magnitudes, although the UGC 2162 magnitudes were from Trujillo et al. (2017). Magnitudes used for calculating the $g - i$ colours and M_* for the Leisman sample were corrected for galactic extinction using the Schlafly & Finkbeiner (2011) values from NED extinction calculator. From Figure 5 we see that UGC 2162 has amongst the smallest R_e of the UDGs with H I detections. However, its $M_{H I}/M_*$ of 9.0 while not as extreme as some Leisman UDGs is above that samples typical value. On the other hand UGC 2162's $g - i$ colour⁵ (0.243) is slightly bluer than most of the Leisman sample, which probably reflects the current enhancement in SFR noted by Trujillo et al. (2017). The H I rich nature of UGC 2162 is also confirmed in comparison with the simulated UDGs from Di Cintio et al. (2017), see Figure 4. This figure shows UGC 2162 to have a smaller R_e and be gas rich compared to an average simulated Di Cintio et al. (2017) UDG.

3.2 H I kinematics

Figure 6 summarises the results from our analysis of UGC 2162 H I kinematics. The upper panel of Figure 6 shows the H I velocity field from medium resolution cube ($30.7'' \times 28.9''$ beam), which has the characteristics of a rotating disc with a moderate rotation velocity and a signature of a warp in the SE. The black contours at the centre of this panel are the two highest H I column density contours from the medium resolution total intensity H I map. These H I contours coincide with the kinematic centre as well as the optical centre of the galaxy. The velocity field of UGC 2162 show no significant sign of recent major interaction. The position velocity (PV) diagram for a slice taken along the H I major axis, position angle (PA) = 307°, is shown in the middle panel of Figure 6 and confirms a rotating disc. A small mass of low density extra-planar H I is seen ~ 15 - 20 arcsec (~ 1 kpc) SE of the kinematic centre in the PV diagram. The lower panel of Figure 6 shows the rotation curve extracted from BBAROLO (Di Teodoro & Fraternali 2015) fit to the medium resolution cube. The figure shows a slowly rising rotation curve which is a common feature for dwarf galaxies. The BBAROLO best fit gives an inclination

⁵ Corrected for galactic extinction.

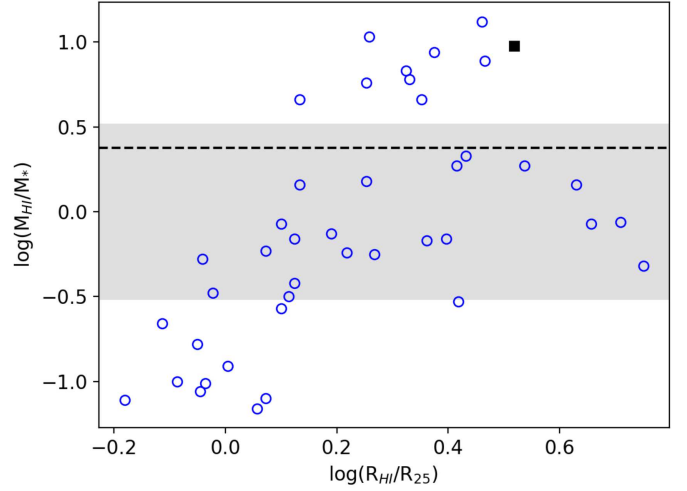


Figure 3. $\log(M_{H I}/M_*)$ v $\log(R_{H I}/R_{25})$: UGC 2162 (black square) and LVHIS local galaxies (limited to galaxies with $M_* < 1 \times 10^8 M_\odot$) from Wang et al. (2017) and Koribalski et al. (2018) - (blue circles). The dashed line is the mean $\log(M_{H I}/M_*)$ for 21 UDGs in the NIHAO simulation (with the shaded area showing its uncertainty) from Di Cintio et al. (2017).

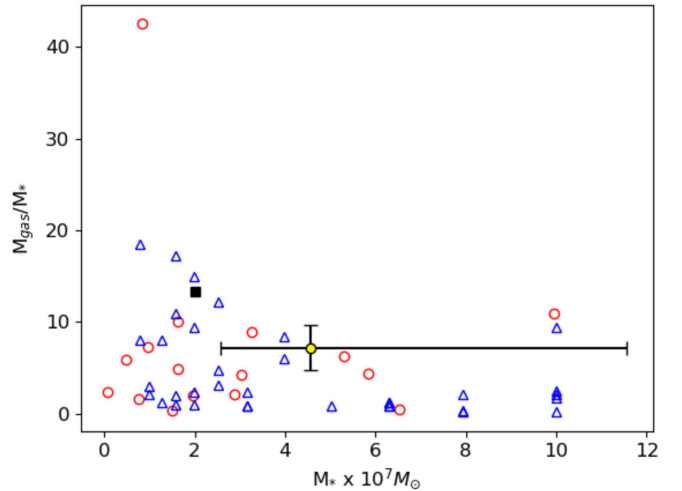


Figure 4. M_{gas}/M_* v M_* : UGC 2162 (black square), LITTLE THINGS dwarf galaxies (red circles) from Oh et al. (2015) and LVHIS local galaxies from Wang et al. (2017) and Koribalski et al. (2018) - (blue triangles). The yellow filled circle is the mean M_{gas}/M_* v M_* for 21 UDGs in the NIHAO simulation from Di Cintio et al. (2017).

of 55.5°, with V_{rot} at the outermost fitted ring, $r = 67.5$ arcsec (4.05 kpc) ~ 25 km s⁻¹. The M_{dyn} enclosed within each ring fitted with BBAROLO is used in section 4.1 to estimate the galaxy's virial mass (M_{vir}). We also estimated the V_{rot} using the H I W_{20} (adjusted for the inclination from the BBAROLO model fit) where $V_{rot} = 0.5 \Delta V$ [km s⁻¹]/sin(i) with $\Delta V = W_{20}$ (50 km s⁻¹) from the GBT spectrum

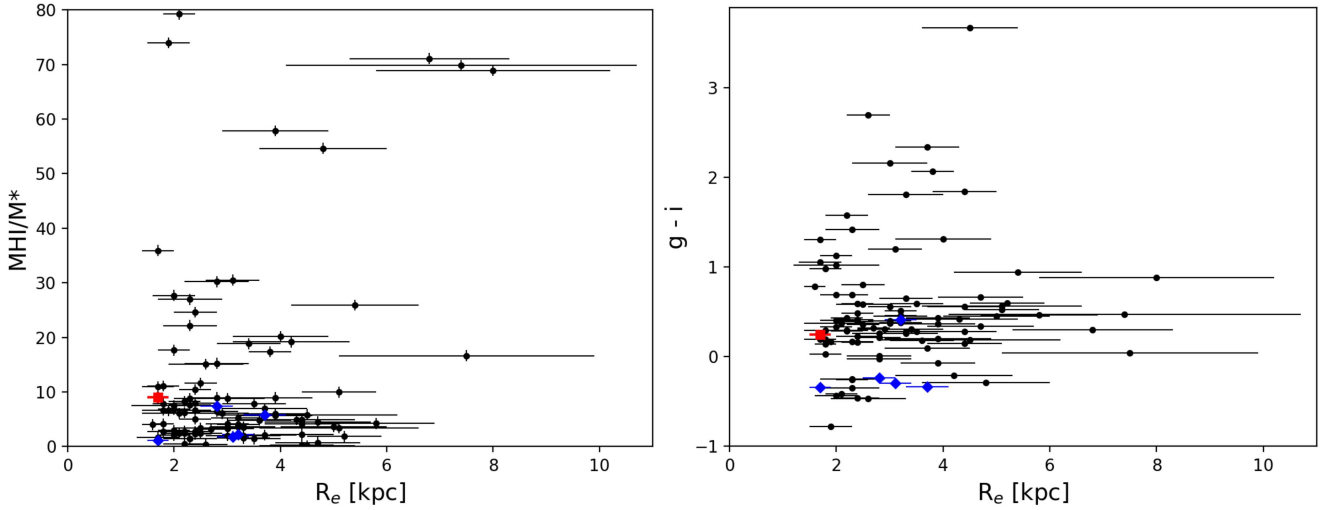


Figure 5. M_{HI}/M_* v R_e UGC 2162 [red square] in comparison with UDG samples with H I detections; H I-bearing ultra-diffuse ALFALFA sources (HUDS) from Leisman et al. (2017) [black dots] and H I mapping from Spekkens and Karunakaran (2018) [blue diamonds].

and $i = 55.5^\circ \pi/180$. This second method gives $V_{\text{rot}} \sim 30.8 \text{ km s}^{-1}$ at the outer edge of the detected H I disk. These values are also used in the section 4.1 analysis.

In Figure 7 we compare the V_{rot} from for UGC 2162 with the V_{rot} derived from model fits to the VLA H I for the LITTLE THINGS dwarf galaxies by Oh et al. (2015). The plot shows that the UGC 2162 $V_{\text{rot}} = 30.8 \text{ km s}^{-1}$, derived from the GBT W_{20} , falls within the range of V_{rot} for LITTLE THINGS with similar M_{HI} and below the LITTLE THINGS median V_{rot} of 39.5 km s^{-1} .

A galaxy's A_{flux} ratio is a measure of the asymmetry in its integrated H I flux density profile (within its W_{20} velocity range) at velocities above and below the galaxy's systemic velocity, V_{HI} . Even isolated late-type galaxies display a scatter of A_{flux} ratio, which is well characterised by a half Gaussian, with its mean equal to 1.0 and a 1σ dispersion of 0.13. This half Gaussian was obtained from a fit to the distribution of A_{flux} values from a sample of AMIGA⁶ isolated galaxies (Espada et al. 2011). The value of an A_{flux} deviating by 1σ from the mean of that distribution is then 1.13. A study by Scott et al. (2018) indicated that A_{flux} is quite sensitive to recent ($\leq 0.7 \text{ Gyr}$) interactions which impact H I disks. For UGC 2162 $A_{\text{flux}} = 1.07 \pm 0.13$, measured from the GBT H I spectrum, which is within the 1σ value from the isolated sample. UGC 2162's H I profile is therefore consistent with a symmetric morphology. Both the H I A_{flux} and the velocity field indicate a relatively unperturbed rotating H I disk which makes it suitable for use in determining the galaxy's M_{dyn} and M_{vir} . Overall UGC 2162's H I kinematics indicate a moderately rotating disk viewed at an inclination of 55.5° . A comparison with the LITTLE THINGS sample of dwarf galaxies indicates its V_{rot} of 30.8 km s^{-1} falls within the range of V_{rot} for LITTLE THINGS galaxies with similar M_{HI} , but below the median V_{rot} for LITTLE THINGS galaxies.

⁶ Analysis of the interstellar Medium of Isolated GALaxies

4 DISCUSSION

The main goals of our H I observations of UDGs are to improve knowledge of the nature of their dark matter halos and to constrain UDG formation scenarios. In this section we consider our results for UGC 2162.

4.1 Dark matter halo of UGC 2162

As a key driver of UDG formation and evolution, their DM mass and its distribution has been debated and investigated using models and globular cluster velocity dispersions observations (e.g., van Dokkum et al. 2016; Toloba et al. 2018) as well as single dish H I spectra (e.g. Trujillo et al. 2017; Spekkens & Karunakaran 2018). Seeing faint UDGs surviving in clusters, van Dokkum et al. (2015a,b) predicted them to be dark matter dominated galaxies. A subsequent velocity dispersion measurement and globular cluster count for DF44 (a Coma cluster UDG, with luminosity $L_v \sim 2 \times 10^8 L_\odot$) indicated a MW size DM halo with $M_h \sim 10^{12} M_\odot$ (van Dokkum et al. 2016). More recent studies show that, while high dynamical to stellar mass ratios are common in UDGs, e.g. VCC1287, DF17 and 18 Coma UDGs, typically dwarf scale halos are inferred (Beasley & Trujillo 2016; Amorisco & Loeb 2016). Zaritsky (2017), using scaling relations, suggested that UDGs may span a range of halo masses between large spirals and dwarf galaxies, though no observations have been carried out to verify these predictions. Additionally, several observational studies of UDGs have used globular cluster velocity dispersions to estimate their DM content (e.g. Beasley et al. 2016; van Dokkum et al. 2018; Toloba et al. 2018). Biases related to the use of globular clusters to determine UDG DM halo masses are discussed in Laporte et al. (2019). However, resolved H I can probe DM halo properties to much larger radii than globular clusters. Therefore, at least for gas rich UDGs H I is better suited to investigating the critical questions of a UDG's DM mass and its distribution.

The H I rotation curves of massive spiral galaxies are observed to initially rise steeply but quickly become flat and remain flat in

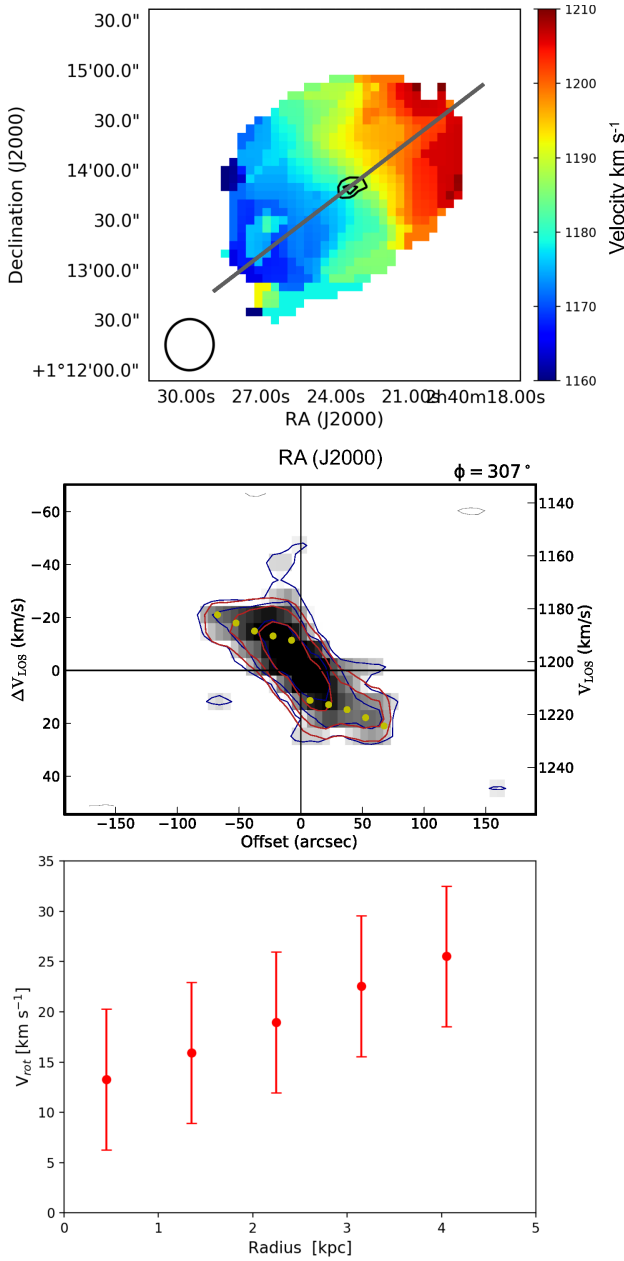


Figure 6. UGC 2162 H I kinematics: *Top:* GMRT velocity field from the medium resolution cube. The two highest column density contours from the medium resolution H I integrated map are shown in black. The PV diagram (panel below) slice PA = 307° is shown with a grey line. *Middle:* PV diagram from a PA = 307° slice. Positive positional offsets are to the NW. The blue contours are from the data and the red are from the BBAROLO best fit model. *Bottom:* Rotation curve derived from the BBAROLO five ring model fit.

the outer regions. In contrast dwarf galaxies’ H I rotation curves are observed to rise more slowly without necessarily flattening out (Di Teodoro & Fraternali 2015) and this is the trend observed in the UGC 2162 H I rotation curve, see Figure 6. We used the V_{rot} and radius for each of the 5 model rings fitted by BBAROLO to the

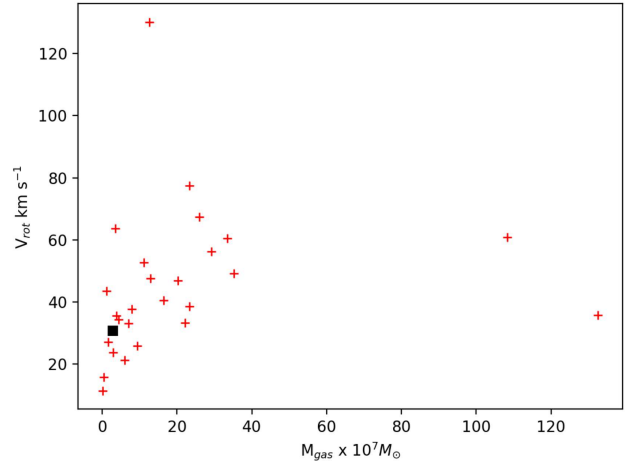


Figure 7. V_{rot} v M_{gas} : UGC 2162 (Black square) and LITTLE THINGS dwarf galaxies (red crosses) from Oh et al. (2015). The UGC 2162, $V_{rot} = 30.8 \text{ km s}^{-1}$ is derived from the GBT W₂₀ in section 3.2. For both UGC 2162 and the LITTLE THINGS galaxies $M_{gas} = 1.4 \times M_{HI}$ with the additional factor to account for molecular gas and He.

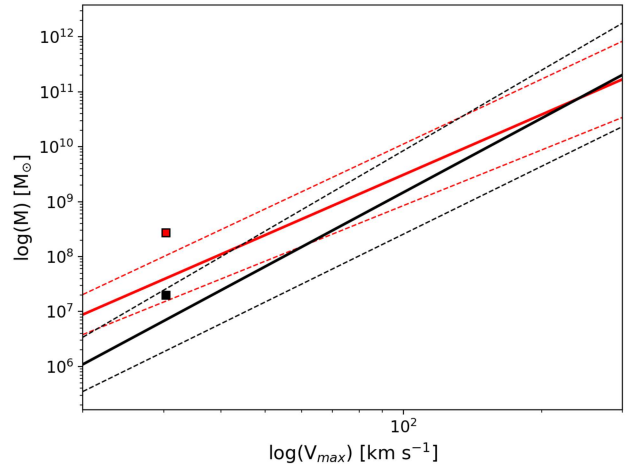


Figure 8. UGC 2162 Tully–Fisher relations: The position of UGC 2162 is shown with a red square relative to the Baryonic Tully–Fisher Relation (red solid line). Also shown is UGC 2162’s position (black square) relative to the Stellar Tully–Fisher Relation (black solid line). The dashed lines in each colour indicate the 1 σ scattered in their respective Tully–Fisher Relation.

medium resolution GMRT H I cube together with equation 1 below to calculate the M_{dyn} enclosed within the radius of each ring:

$$M_{dyn} = V_{rot}^2 r_{HI} / G [M_{\odot}] \quad (1)$$

For UGC 2162 the BBAROLO model ring with the largest radius from the H I kinematic centre was at $r_{HI} = 67.5 \text{ arcsec}$ ($\sim 4.05 \text{ kpc}$). Using this ring’s H I extent and $V_{rot} = 25.5 \text{ km s}^{-1}$, we estimate the dynamical mass (M_{dyn}) within the inner 4.05 kpc using equation 1 as $\sim 0.6 \times 10^9 M_{\odot}$. Additionally, we calculated $M_{dyn} = 1.14$

$^{+0.57}_{-0.47} \times 10^9 M_{\odot}$ enclosed within the $R_{HI} \sim 86$ arcsec (5.2 kpc), estimated from the low resolution GMRT map and $V_{rot} = 30.8 \text{ km s}^{-1}$ derived in Section 3.2 from the GBT W_{20} . Our M_{dyn} value ($1.14 \times 10^9 M_{\odot}$) enclosed within the 5.2 kpc R_{HI} is only about 25% of the $M_{dyn} = 4.6 \times 10^9 M_{\odot}$ based on a guessed at, but similar, R_{HI} reported in Trujillo et al. (2017). The difference is principally due to their adoption of an inclination corrected $V_{rot} = 64 \text{ km s}^{-1}$ based on a HIPASS $W_{20} = 89 \text{ km s}^{-1}$ from Meyer et al. (2004). The Meyer value is nearly twice the GBT W_{20} of $50 \pm 2 \text{ km s}^{-1}$ we have adopted. But Table 2 shows our re-measurement of the HIPASS W_{20} is in agreement, within the uncertainties, with both the GBT and GMRT W_{20} values.

Figure 9 shows, with red open circles, the M_{dyn} enclosed within the five BBAROLO model radii of 7.5", 22.5", 37.5", 52.5" and 67.5" (0.45, 1.35, 2.25, 3.15 and 4.05 kpc) from the H I kinematic centre using equation 1. The $M_{dyn} = 1.14^{+0.57}_{-0.47} \times 10^9 M_{\odot}$ enclosed within the $R_{HI} \sim (5.2 \text{ kpc})$ is shown in the figure with a black square. The figure also shows Navarro–Frenk–White (NFW) model⁷ cumulative masses for DM halos with $M_{200} = 5 \times 10^{10} M_{\odot}$ (red dashed curve) and $M_{200} = 8.8 \times 10^{10} M_{\odot}$ (black solid curve). The respective V_{max} from these halo models are 51.1 km s^{-1} and 64.2 km s^{-1} with the respective R_{200s} of 228 kpc and 275 kpc. A concentration parameter = 2 was used for both NFW models. The two NFW models fit the M_{dyn} enclosed within ring radii derived from BBAROLO and the low resolution H I map disk edge radius, provide a likely range for the UGC 2162 DM halo properties. Figure 10 shows the inferred M_{200} for UGC 2162 (mean from two NFW halo models) = $6.9 \times 10^{10} M_{\odot}$, which is a factor of three higher than the median M_{200} ($2.1 \times 10^{10} M_{\odot}$) for the LITTLE THINGS dwarf galaxies from model fits carried out by Oh et al. (2015). Additionally, UGC 2162’s rotation curve is consistent with the slowly rising rotation curves observed in dwarf and LSB galaxies (e.g. Oh et al. 2015).

To summarise, we estimate the UGC 2162’s M_{dyn} is $\sim 1.14 \times 10^9 M_{\odot}$ within the R_{HI} (5.2 kpc), derived from the low resolution H I map. Halo model fits to both this and M_{dyn} derived from BBAROLO ring model fits infer M_{200} in the range $5.0 - 8.8 \times 10^{10} M_{\odot}$, which is slightly higher than the median for LITTLE THINGS galaxies. UGC 2162 also displays a slowly rising H I rotation curve, typical of dwarf galaxies. UDGs encompass a range of different types of galaxies from dark matter dominated (eg. DF44: van Dokkum et al. (2016) to lacking in dark matter (eg. 1052-DF2: Danieli et al. (2019)). In that spectrum of galaxies, a comparison of the physical properties, M_{200} , H I velocity curve profiles and V_{rot} reported for LITTLE THINGS dwarf galaxies, lead us to conclude that the baryonic component of UGC 2162 is inhabiting a dark matter halo with a mass and profile characteristic of a dwarf galaxy.

4.2 Formation scenario

As noted in Section 1, there are multiple hypotheses in the literature regarding formation of UDGs. It is also not clear if an umbrella term UDG should be used for these galaxies which may be in reality a collection of galaxies of all sizes, morphologies and stages of evolution with the only common factor being their extremely faint central surface brightness. We discuss here possible formation scenarios of the dwarf UDG, UGC 2162.

As shown in Figure 4 and described in Section 3.1 the M_{gas}/M_{*}

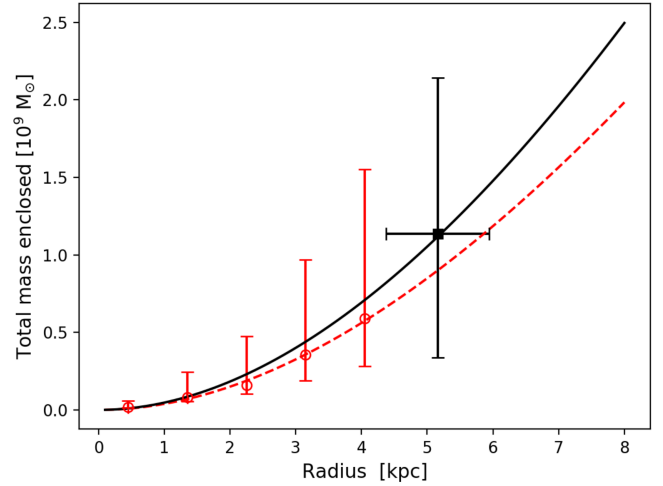


Figure 9. UGC 2162: M_{dyn} interior to the five ring BBAROLO H I model fits (red open circles) and M_{dyn} derived from the R_{HI} from low resolution GMRT H I map and W_{20} (black square). Also shown are NFW model cumulative masses for DM halos with $M_{200} = 5 \times 10^{10} M_{\odot}$ (red dashed curve) and $M_{200} = 8.8 \times 10^{10} M_{\odot}$ (black solid curve). The concentration parameter = 2 for both NFW models.

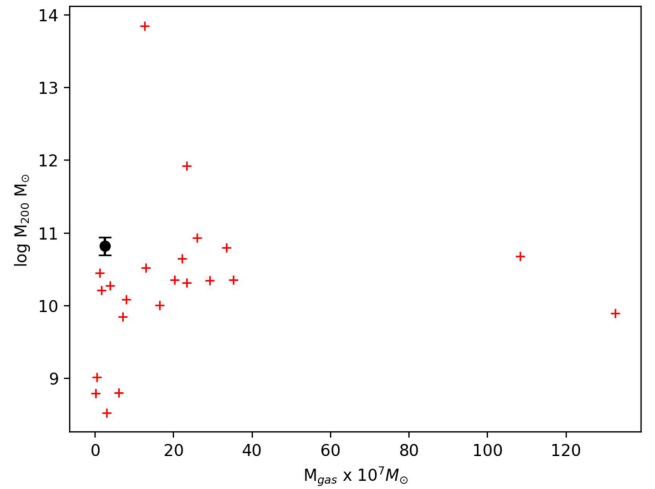


Figure 10. Mean M_{200} from the two NFW models from section 4.1 for UGC 2162 (black circle) and model fits to LITTLE THINGS dwarf galaxies from Oh et al. (2015) (red crosses) v M_{gas} .

for UGC 2162 is a factor 3 higher than the median ratio for the LITTLE THINGS dwarf galaxies of similar M_{gas} . We plot in Figure 8 the UGC 2162 baryonic and stellar masses vs V_{max} compared to both Baryonic and Stellar Tully–Fisher relations from McGaugh et al. (2000); Torres-Flores et al. (2011). For this plot we made the same assumption about the relation of M_{gas} to M_{HI} as we did in Section 4.1, i.e. $M_{gas} = 1.4 \times M_{HI}$. The plot shows that while UGC 2162’s

⁷ Halotools (Hearin et al. 2017)

baryonic mass falls above the upper 1σ uncertainty for Baryonic Tully-Fisher relation (BTFR), its stellar mass is within 1σ uncertainty for the Stellar Tully Fisher relation. No strong conclusion should be drawn based on this as the mass estimates for an individual galaxy usually has large uncertainties. But, this result marginally reinforces the indications that UGC 2162 is gas rich relative to its stellar mass, suggesting that some mechanism has in the past suppressed its SF and star formation efficiency (SFE) to much lower levels than its currently elevated star formation rate (SFR) of $0.01 M_{\odot} \text{ yr}^{-1}$ estimated by Trujillo et al. (2017). Wong et al. (2016) argues that the secular evolution of a combination of disk stability and disk hydrostatic pressure is the primary driver of the observed H I based star formation efficiency (SFE_{HI}). They find angular momentum to have only a secondary effect, concluding that for stable rotating H I disks the scatter in the SFE_{HI} from variation in angular momentum is of the order of a factor of ~ 2 . UGC 2612's SFE_{HI} is a factor of 4 below the average SFE_{HI} of the Wong et al. (2016) HIPASS-selected sample of SF galaxies. This indicates additional mechanisms may have operated over extended periods (Gyrs) to suppress its SFE_{HI} or alternatively it recently acquired a substantial fraction of its current H I mass.

Although UGC 2162 is part of a loose group of galaxies, it is currently fairly isolated with respect to its nearest physical companion of similar or larger mass (SDSS J023848.50+003114.2) projected ~ 175 kpc away. The H I images and kinematics of UGC 2162 show no clear signs of recent major interaction, harassment or environment related effects that could have led to a major gas loss or significantly influence its morphology. On its own the presence of UGC 2162's H I warp does not necessarily indicate a recent interaction as H I warps are also seen in isolated galaxies which have been free from major tidal interaction for several Gyrs, e.g. (Sengupta et al. 2012; Portas et al. 2011; Scott et al. 2014), where they have been attributed to secular processes and interactions with minor satellites. Based on the projected distance to its nearest neighbour and the relative velocity of $\sim 277 \text{ km s}^{-1}$, UGC 2162 could have suffered a tidal interaction ~ 0.3 Gyr ago with its nearest neighbour (\sim less than the galaxy rotation period⁸), which could conceivably be responsible for both the H I disk warp and currently enhanced SFR. But we argue that if such an interaction did take place, the galaxy's current state implies that it was most likely a minor flyby that did not sufficiently affect UGC 2162's morphology to induce its transformation to an UDG. According to the modelling by (Holwerda et al. 2011), HI morphology asymmetries from major merger interactions remain detectable for between 0.4 to 0.7 Gyrs. So presumably for UGC 2162 an encounter with a similar or larger sized or larger group member would remain obvious in the HI morphology for at least that time. In UGC 2162 we do not see any tidal remnants, tidal features or any gas deficiency, which supports our argument against a recent major interaction. Hence, any process that drove UGC 2162 to become a UDG is most likely a long term internal or secular one. Figure 7 compares the V_{rot} of UGC 2162 to those of LITTLE THINGS dwarfs of similar H I mass and we see that UGC 2162 is a slow rotator for its H I mass, in agreement with the Tully-Fisher analysis.

The estimated halo spin parameter (λ) using Hernandez et al. (2007)'s estimator for spiral galaxies gives a moderate λ value of 0.1 for UGC 2162. Compared to the higher spin UDGs in Leisman et al. (2017) or Spekkens & Karunakaran (2018),

⁸ $T_{rot} = 1.45 \text{ Gyr} = 2\pi R_{HI}/V_{rot}$ where $V_{rot} = 0.5\Delta W_{20}/\sin(i)$, $W_{20} = 50 \text{ km s}^{-1}$ and $i = 55^{\circ}$

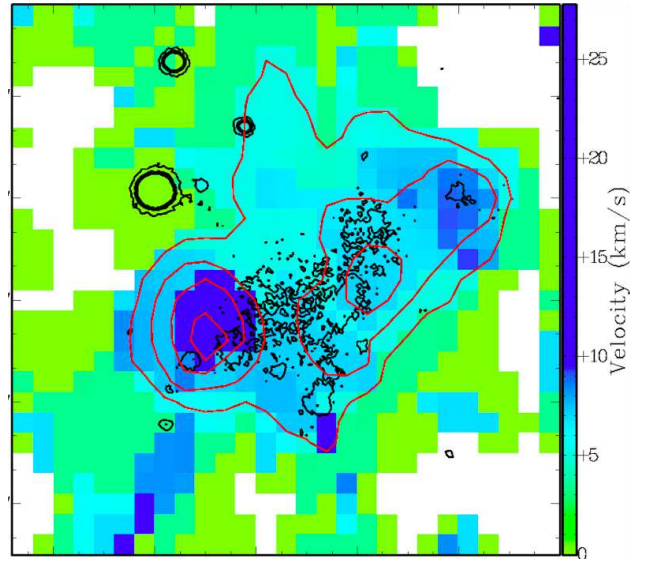


Figure 11. UGC 2162 H I –stellar correlation near optical center: integrated H I contours (high resolution, red) and star forming regions (SDSS g-band in black contours) plotted on H I velocity dispersion (in blue/cyan) map.

UGC 2162 seems to qualify as a moderate to lower spin galaxy. However, we prefer not to make any claims about halo spin of UGC 2162 as none of the assumptions made to estimate λ in Hernandez et al. (2007) and Spekkens & Karunakaran (2018) matches UGC 2162's properties. Instead we prefer to emphasize that most of UGC 2162's properties strongly resemble those of normal dwarf galaxies (e.g. LITTLE THINGS sample) and more importantly the galaxy does not exhibit an abnormally extended disk compared to its DM halo mass to invoke a high spin halo formation scenario for it. From this we infer that for UGC 2162, we can safely rule out the UDG formation scenario involving high spin halos proposed by Amorisco & Loeb (2016).

The galaxy shows blue star forming regions near the optical centre and the highest UGC 2162 H I column densities ($1.0 - 1.3 \times 10^{21} \text{ cm}^{-2}$) in the high resolution map approximately coincide with these star forming zones in the SDSS background image (Figure 1). UGC 2162 also has a faint optical disk revealed in the IAC stripe82 g, r, i composite image in Figure 1 of Trujillo et al. (2017) of radius ~ 60 arcsec with a $\mu_g > 26 \text{ mag arcsec}^{-2}$ at the disk edge. Fig 11 shows the highest column density contours (in red) from the high resolution H I map overlaid on the high resolution H I velocity dispersion map. The projected positions of the highest density H I and H I velocity dispersion maximum in the Figure coincide and are offset ~ 20 arcsec (1.2 kpc) to the SE of the optical centre. Additionally, there is evidence of diffuse extra-planar H I in the pv diagram (Figure 6) coinciding with the highest H I dispersion zone. This may indicate some moderate to low level SF related outflow, but the highly disruptive past outflows proposed by van Dokkum et al. (2016) and Di Cintio et al. (2017) to explain the origin of UDGs can be ruled out in this case, given the galaxy is currently undergoing a heightened level of SF and its low accumulated stellar mass.

5 SUMMARY AND CONCLUDING REMARKS

Overall the H I morphology and kinematics of UDG 2162 indicates a rather symmetric H I disk within a DM halo with a mass and profile typical of dwarf galaxies. However, the H I disk contains a warp and a moderate, currently elevated, SFR of $0.01 M_{\odot}$ which might be attributable to an interaction with a fellow group member in last ~ 0.3 Gyr. Comparing UGC 2162 to samples of UDGs with H I detections show it to have amongst the smallest R_e with its M_{HI}/M_* being higher and $g-i$ colour bluer than typical values in those samples. The galaxy is classified as UDG but our investigation could not unambiguously connect its current state to any of the proposed formation scenarios in the literature. On the other hand we could rule out some of the most common proposed scenarios and infer the following: 1) UGC 2162's DM halo is a dwarf halo typical of normal dwarf galaxies 2) the similarity of UGC 2162's properties to those of the LITTLE THINGS sample does not support a scenario requiring abnormally high spin 3) the environment and H I content of the galaxy does not indicate a formation scenario depending on a recent interaction or environmental assistance; 4) we did not find evidence of recent or past highly disruptive SF driven outflows. A detailed modelling of the galaxy's star formation history may throw more light on how this galaxy formed.

6 ACKNOWLEDGEMENTS

We thank the staff of the *GMRT* who have made these observations possible. The *GMRT* is operated by the National Centre for Radio Astrophysics of the Tata Institute of Fundamental Research. TS acknowledge support by Fundação para a Ciência e a Tecnologia (FCT) through national funds (UID/FIS/04434/2013), FCT/MCTES through national funds (PIDDAC) by this grant UID/FIS/04434/2019 and by FEDER through COMPETE2020 (POCI-01-0145-FEDER-007672). TS also acknowledges the support by the fellowship SFRH/BPD/103385/2014 funded by FCT (Portugal) and POPH/FSE (EC). TS additionally acknowledges support from DL 57/2016/CP1364/CT0009. This work was supported by FCT/MCTES through national funds (PIDDAC) by this grant PTDC/FIS-AST/29245/2017. Support for this work was provided by the National Research Foundation of Korea to the Center for Galaxy Evolution Research (No. 2010-0027910) and NRF grant No. 2018R1D1A1B07048314. This research has made use of the NASA/IPAC Extragalactic Database (NED) which is operated by the Jet Propulsion Laboratory, California Institute of Technology, under contract with the National Aeronautics and Space Administration. This research has made use of the Sloan Digital Sky Survey (SDSS). Funding for the SDSS and SDSS-II has been provided by the Alfred P. Sloan Foundation, the Participating Institutions, the National Science Foundation, the U.S. Department of Energy, the National Aeronautics and Space Administration, the Japanese Monbukagakusho, the Max Planck Society, and the Higher Education Funding Council for England. The SDSS Web Site is <http://www.sdss.org/>. This research made use of APLpy, an open-source plotting package for Python hosted at <http://aplpy.github.com>. This research made use of APLpy, an open-source plotting package for Python (Robitaille & Bressert 2012). The Parkes telescope is part of the Australia Telescope which is funded by the Commonwealth of Australia for operation as a National Facility managed by CSIRO.

REFERENCES

- Amorisco N. C., Loeb A., 2016, *MNRAS*, **459**, L51
- Baars J. W. M., Genzel R., Pauliny-Toth I. I. K., Witzel A., 1977, *A&A*, **61**, 99
- Beasley M. A., Trujillo I., 2016, *ApJ*, **830**, 23
- Beasley M. A., Romanowsky A. J., Pota V., Navarro I. M., Martinez Delgado D., Neyer F., Deich A. L., 2016, *ApJ*, **819**, L20
- Bell E. F., McIntosh D. H., Katz N., Weinberg M. D., 2003, *ApJS*, **149**, 289
- Blanton M. R., Hogg D. W., Bahcall N. A., Brinkmann J., Britton M., Connolly A. J., Csabai I., Fukugita M., 2003, *ApJ*, **592**, 819
- Broeils A. H., Rhee M.-H., 1997, *A&A*, **324**, 877
- Carleton T., Errani R., Cooper M., Kaplinghat M., Peñarrubia J., Guo Y., 2019, *MNRAS*, **485**, 382
- Danieli S., van Dokkum P., Conroy C., Abraham R., Romanowsky A. J., 2019, *ApJ*, **874**, L12
- Di Cintio A., Brook C. B., Dutton A. A., Macciò A. V., Obreja A., Dekel A., 2017, *MNRAS*, **466**, L1
- Di Teodoro E. M., Fraternali F., 2015, *MNRAS*, **451**, 3021
- Espada D., Verdes-Montenegro L., Huchtmeier W. K., Sulentic J., Verley S., Leon S., Sabater J., 2011, *A&A*, **532**, A117
- Haynes M. P., Giovanelli R., 1984, *AJ*, **89**, 758
- Hearin A. P., et al., 2017, *AJ*, **154**, 190
- Hernandez X., Park C., Cervantes-Sodi B., Choi Y.-Y., 2007, *MNRAS*, **375**, 163
- Holwerda B. W., Pirzkal N., Cox T. J., de Blok W. J. G., Weniger J., Bouchard A., Blyth S.-L., van der Heyden K. J., 2011, *MNRAS*, **416**, 2426
- Koribalski B. S., et al., 2018, *MNRAS*, **478**, 1611
- Laporte C. F. P., Agnello A., Navarro J. F., 2019, *MNRAS*, **484**, 245
- Leisman L., et al., 2017, *ApJ*, **842**, 133
- McGaugh S. S., Schombert J. M., Bothun G. D., de Blok W. J. G., 2000, *ApJL*, **533**, L99
- Meyer M. J., et al., 2004, *MNRAS*, **350**, 1195
- Oh S.-H., et al., 2015, *AJ*, **149**, 180
- Portas A., et al., 2011, *ApJL*, **739**, L27
- Robitaille T., Bressert E., 2012, APLpy: Astronomical Plotting Library in Python, Astrophysics Source Code Library (ascl:1208.017)
- Román J., Trujillo I., 2017, *MNRAS*, **468**, 4039
- Schlafly E. F., Finkbeiner D. P., 2011, *ApJ*, **737**, 103
- Scott T. C., et al., 2014, *A&A*, **567**, A56
- Scott T. C., Brinks E., Cortese L., Boselli A., Bravo-Alfaro H., 2018, *MNRAS*, **475**, 4648
- Sengupta C., et al., 2012, *A&A*, **546**, A95
- Spekkens K., Karunakaran A., 2018, *ApJ*, **855**, 28
- Springob C. M., Haynes M. P., Giovanelli R., Kent B. R., 2005, *ApJS*, **160**, 149
- Toloba E., et al., 2018, *ApJL*, **856**, L31
- Torres-Flores S., Epinat B., Amram P., Plana H., Mendes de Oliveira C., 2011, *MNRAS*, **416**, 1936
- Trujillo I., Roman J., Filho M., Sánchez Almeida J., 2017, *ApJ*, **836**, 191
- Wang J., et al., 2017, *MNRAS*, **472**, 3029
- Wittmann C., et al., 2017, *MNRAS*, **470**, 1512
- Wong O. I., Meurer G. R., Zheng Z., Heckman T. M., Thilker D. A., Zwaan M. A., 2016, *MNRAS*, **460**, 1106
- Yagi M., Koda J., Komiyama Y., Yamanoi H., 2016, *ApJS*, **225**, 11
- Yozin C., Bekki K., 2015, *MNRAS*, **452**, 937
- Zaritsky D., 2017, *MNRAS*, **464**, L110
- van Dokkum P. G., Abraham R., Merritt A., Zhang J., Geha M., Conroy C., 2015a, *ApJL*, **798**, L45
- van Dokkum P. G., et al., 2015b, *ApJL*, **804**, L26
- van Dokkum P., et al., 2016, *ApJL*, **828**, L6
- van Dokkum P., et al., 2018, *ApJL*, **856**, L30
- van der Burg R. F. J., et al., 2017, *A&A*, **607**, A79